

# Two-dimensional crystals of Rydberg excitations in a resonantly driven lattice gas

David Petrosyan

*Institute of Electronic Structure and Laser, FORTH, GR-71110 Heraklion, Crete, Greece*

(Dated: March 11, 2019)

The competition between resonant optical excitation of Rydberg states of atoms and their strong, long-range van der Waals interaction results in spatial ordering of Rydberg excitations in a two-dimensional lattice gas, as observed in a recent experiment of Schauß *et al.* [Nature **491**, 87 (2012)]. Here we use semiclassical Monte Carlo simulations to obtain stationary states for hundreds of atoms in finite-size lattices. We show the formation of regular spatial structures of Rydberg excitations in a system of increasing size, and find highly sub-Poissonian distribution of the number of Rydberg excitations characterized by a large negative value of the Mandel  $Q$  parameter which is nearly independent of the system size.

PACS numbers: 37.10.Jk, 32.80.Ee, 75.30.Fv

## I. INTRODUCTION

Cold atoms in optical lattices represent a remarkably clean and controllable systems to simulate and study many-body physics [1]. A crucial ingredient for realizing various phases of matter is to have access to interactions with different strength and range. The interaction between the ground-state atoms in a lattice is typically short range (on-site) and can be tuned relative to the (inter-site) tunneling energy to realize the Hubbard's model transition from the superfluid to the Mott insulator phase with precisely one atom per lattice site [2]. Second order tunneling [3] can translate into an effective nearest-neighbor interaction which allows the realization of the Heisenberg spin or extended Hubbard models [4, 5]. Dipolar interactions [6] between atoms with large magnetic moment or between polar molecules have still longer range. But atoms excited to the Rydberg states exhibit unprecedented magnitude and range of dipole-dipole or van der Waals interactions [7–9]. Dressing ground state atoms by the Rydberg state with an off-resonant laser field can thus lead to an effective long-range interaction [10–13].

An alternative approach is to explore resonant coupling of the ground state atoms to the highly excited Rydberg states [9]. The interaction between the atoms in Rydberg states translates into the level shifts of multiple Rydberg excitations which are therefore suppressed in dense atomic ensembles [14–19]. Thus, within a small volume, where the interatomic interaction energies exceed the excitation linewidth of the Rydberg state, a single Rydberg atom blocks the excitation of all the other atoms [20–26]. Larger atomic ensembles can accommodate more Rydberg excitations which effectively repel each other so that no two Rydberg atoms can be closer than the blockade distance [27–29]. Simultaneously, the total number of excitations within the ensemble exhibits reduced fluctuations [30–32].

Spatial correlations and crystallization of Rydberg excitations have recently attracted many theoretical investigations [12, 13, 33–49]. A recent experiment of Schauß *et al.* [29] have spectacularly demonstrated spatial or-

dering of Rydberg excitations of resonantly driven atoms in a two-dimensional (2D) optical lattice with circular boundaries. In that experiment, the lifetime of the Rydberg state ( $\tau_r \sim 25 \mu\text{s}$ ) and the coherence time of the atomic polarization ( $\tau_z \sim 10 \mu\text{s}$ ) were much longer than the duration ( $t \sim \mu\text{s}$ ) of the optical excitation pulses. Hence, neglecting the relaxations, numerical simulations of the coherent excitation dynamics of many-body system well reproduced the experimental observations [29]. The purpose of the present study is to obtain and characterize the many-body stationary state attained by the dissipative system upon a long-time (continuous) excitation. To that end, we employ an iterative Monte Carlo sampling algorithm [49] to simulate the distribution of Rydberg excitations of the atoms in a 2D lattice of variable size. Similarly to [29], we obtain spatially ordered patterns formed by definite numbers of Rydberg excitations, while the probability distribution of the excitation numbers is very narrow (highly sub-Poissonian) characterized by a large negative value of the Mandel  $Q$  parameter [50] which is consistent with the observations in [30–32]. With increasing the size (diameter  $d$ ) of the cloud, while keeping the atomic density fixed, the mean number of Rydberg excitations grows ( $\propto d^{5/3}$ ), but its distribution remains sub-Poissonian with nearly constant  $Q \approx -0.84$ . Concurrently, the Rydberg excitations tend to arrange in regular spatial shell structures.

A few words on the numerical procedure employed below are in order now. The semiclassical Monte Carlo algorithm and closely related methods were previously used in several publications [32, 49, 51–53]. Its essence is to treat each atom separately in a potential generated by all the other atoms excited to the Rydberg state, while neglecting the inter-atomic coherences (entanglement). This approximation is not exact, unless the dephasing rate is larger than the Rabi frequency of the driving field (which is not the case in [29]), but it becomes better with increasing the relaxation, or dephasing, of the atomic polarization [49]. As discussed in more detail at the end of the paper, however, the steady state obtained here approximates the state of the system resulting after just a few  $\mu\text{s}$  driving [29] qualitatively correctly [54].

## II. THE MONTE CARLO ALGORITHM

Let us start by recalling the properties of a single two-level atom driven by a laser field with Rabi frequency  $\Omega$  and detuning  $\delta$  on the transition from the ground state  $|g\rangle$  to the excited (Rydberg) state  $|r\rangle$ . We denote by  $\Gamma_r$  the decay rate of the excited state population  $\langle\hat{\sigma}_{rr}\rangle$ , and by  $\Gamma_z$  the relaxation rate of atomic polarization  $\langle\hat{\sigma}_{rg}\rangle$ , where  $\hat{\sigma}_{\mu\nu} \equiv |\mu\rangle\langle\nu|$  is the projection ( $\mu = \nu$ ) or transition ( $\mu \neq \nu$ ) operator of the atom. The steady-state population of the Rydberg state is then a Lorentzian function of detuning  $\delta$  [55],

$$\langle\hat{\sigma}_{rr}\rangle = \frac{\Omega^2}{2\Omega^2 + \frac{\Gamma_r}{2\gamma_{rg}}(\gamma_{rg}^2 + \delta^2)}, \quad (1)$$

with the width  $w \simeq 2\Omega\sqrt{\gamma_{rg}/\Gamma_r}$ , where  $\gamma_{rg} \equiv \frac{1}{2}\Gamma_r + 2\Gamma_z$  and we assume strong driving  $\Omega^2 > \Gamma_r\gamma_{rg}$  (or weak decay  $\Gamma_r < \Omega^2/\gamma_{rg}$ ). On resonance,  $\delta \ll w$ , the population saturates to  $\langle\hat{\sigma}_{rr}\rangle \rightarrow \frac{1}{2}$ .

Atoms in the Rydberg state  $|r\rangle$  interact pairwise via the van der Waals (vdW) potential,  $\hbar\Delta(z) = \hbar C_6/z^6$ , where  $C_6$  is the vdW coefficient and  $z$  is the interatomic distance [56]. Hence, given an atom  $i$  in state  $|r\rangle$ , it will induce a level shift  $\Delta(z_{ij})$  of another atom  $j$ , which effectively translates into the detuning  $\delta$ . When  $\Delta(z_{ij}) \gtrsim w$ , the transition  $|g\rangle \rightarrow |r\rangle$  of atom  $j$  is non-resonant and its Rydberg excitation is blocked by atom  $i$ , which is the essence of the dipole blockade [8, 20]. We can therefore define the blockade distance  $d_b$  via  $\Delta(d_b) = w$  which yields  $d_b = \sqrt[6]{C_6/w}$ .

Our aim is to obtain the stationary distribution of Rydberg excitations of  $N \gg 1$  atoms in a 2D lattice. Exact quantum mechanical solution of the density matrix equations for realistically large  $N \sim 10^2 - 10^3$  is not possible due to the exponentially large in  $N$  Hilbert space of the system. Numerical simulations of unitary dynamics for  $N \lesssim 400$  atoms in a truncated Hilbert space were presented in [29], while dissipative dynamics and the steady state for  $N \lesssim 50$  atoms was studied in [54] using the quantum stochastic wavefunctions approach. Here we make a semiclassical approximation which discards quantum correlations between the atoms but preserves classical  $N$ -body correlations. Its validity hinges on the assumption of strong dephasing  $\Gamma_z \gtrsim \Omega$  which suppresses intra- and interatomic coherences and disentangles the atoms [49]. Each atom  $j$  then behaves as a driven two-level system of Eq. (1) but with the detuning  $\delta$  determined by operator  $\hat{S}_j \equiv \sum_{i \neq j}^N \hat{\sigma}_{rr}^i \Delta(z_{ij})$  which describes the total interaction-induced shift of its level  $|r\rangle$  involving the contributions of all the other Rydberg atoms  $\hat{\sigma}_{rr}^i$ .

We employ the procedure described in [49] to generate the stationary distribution of Rydberg excitations of many atoms  $N$  in a self-consistent way. The algorithm performs an iterative Monte Carlo sampling of  $\{\hat{\sigma}_{rr}^j\}$  for an ensemble of  $N$  atoms, in the spirit of the Hartree-Fock method. We first initialize all the atoms in, e.g.,

the ground state,  $\hat{\sigma}_{gg}^j \rightarrow 1 \forall j \in [1, N]$ . Then, at every step, for each atom  $j$ , we set  $\hat{\sigma}_{rr}^j \rightarrow 1$  or 0 with the probability determined by its current Rydberg state population  $\langle\hat{\sigma}_{rr}^j\rangle$ . In turn, the thus constructed binary configuration of Rydberg excitations  $\{\hat{\sigma}_{rr}^i\} \rightarrow \{0, 1, 0, 0, \dots\}$  determines the level shift  $\hat{S}_j$  (equivalent to detuning  $\delta$ ) of atom  $j$  when evaluating  $\langle\hat{\sigma}_{rr}^j\rangle$ . We continuously iterate this procedure, sifting repeatedly through every atom in the potential generated by all the other atoms. We thus generate a large number ( $\sim 10^6$ ) of configurations  $\{\hat{\sigma}_{rr}^j\}$  from which we obtain the averaged probability distribution  $\bar{\sigma}_{rr}^j$  of Rydberg excitations and their correlations  $\hat{\sigma}_{rr}^i \hat{\sigma}_{rr}^j$ , as well as the probabilities  $p_R(n)$  of  $n$  Rydberg excitations and their spatial patterns.

Note that in the experiment, after preparing the atoms in the ground state  $|g\rangle$  and exciting them with a laser, one performs projective measurements  $\{\hat{\sigma}_{rr}^j\}$  of Rydberg excitations [29]. Every experimental sequence then results in a particular configuration  $\{\hat{\sigma}_{rr}^j\} \rightarrow \{0, 0, 1, 0, \dots\}$ , and averaging over many such experimental sequences yields the Rydberg excitation probabilities for individual atoms or the whole ensemble. The Monte Carlo sampling of the excitation configurations thus closely imitates the experiment.

## III. RESULTS OF NUMERICAL SIMULATIONS

In our simulations, we use the parameters similar to those in the experiment [29], with the exception of a larger relaxation rate  $\Gamma_z$ . We thus take a 2D lattice of cold  $^{87}\text{Rb}$  atoms whose ground state  $|g\rangle \equiv 5S_{1/2}|F=2, m_F=-2\rangle$  is coupled to the Rydberg state  $|r\rangle \equiv 43S_{1/2}$  by a two-photon transition with the Rabi frequency  $\Omega/2\pi = 100$  kHz. The decay rate of  $|r\rangle$  is  $\Gamma_r = 0.065\Omega \simeq 40$  kHz and we assume large enough coherence relaxation rate  $\Gamma_z = \Omega \simeq 630$  kHz (in the experiment  $\Gamma_z \simeq 160$  kHz, stemming from the two-photon laser linewidth  $\sim 70$  kHz and residual decay  $\sim 90$  kHz of the atomic intermediate state to the ground state [29]). The resulting excitation linewidth of  $|r\rangle$  is  $w/2\pi \simeq 0.8$  MHz. With the vdW coefficient  $C_6/2\pi \simeq 2.45$  GHz  $\mu\text{m}^6$  [56] the corresponding blockade distance is  $d_b \simeq 3.81\mu\text{m}$ . We performed numerical simulations for various diameters  $d$  of the circular boundaries enclosing the 2D lattice of atoms at constant density (fixed lattice spacing  $a = 532$  nm [29]).

In Fig. 1 we present the results of simulations for  $d = (1, 2, 3, 4)d_b$ . In part (a) of each panel, we show the Rydberg excitation probabilities  $\bar{\sigma}_{rr}$  averaged over all the configurations for a given diameter  $d$  of the atomic cloud. The spatial distribution of Rydberg excitations is rotationally symmetric, with the largest probabilities at the boundary of the cloud. With increasing the system size, however, we observe a formation of spatial shell structure of Rydberg excitations [the inner ring in Fig. 1(a4)].

In Figs. 1(b1-b4), we show the mean number of Ry-

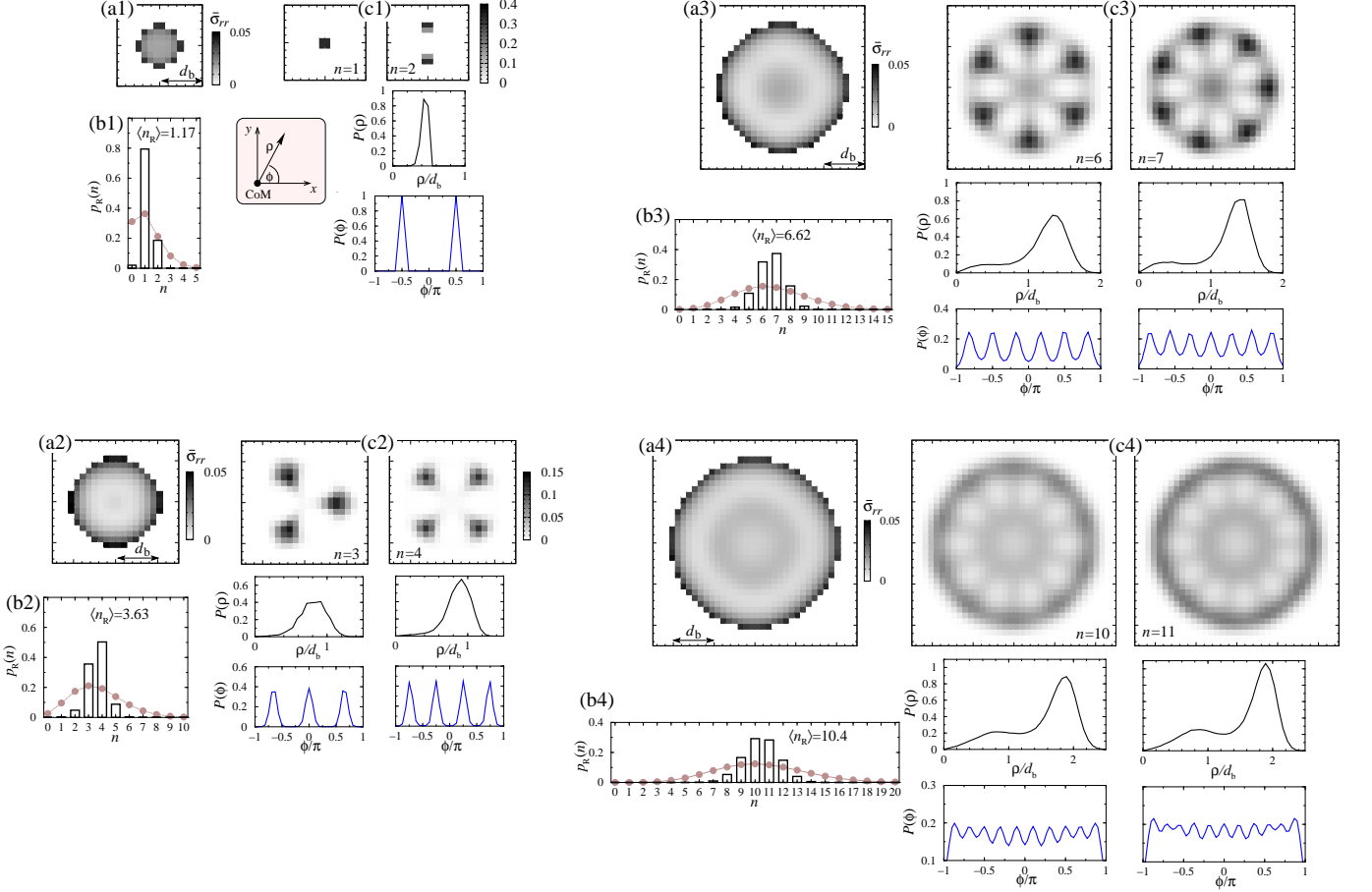


FIG. 1. Rydberg excitations of a resonantly-driven ensemble of  $N = (44, 188, 401, 688)$  atoms in a 2D lattice of diameter  $d = (1, 2, 3, 4)d_b$ , respectively. (a1-a4) Average spatial distribution of Rydberg excitation probabilities  $\bar{\sigma}_{rr}$ ; each pixel corresponds to a single atom/lattice site. (b1-b4) Probabilities  $p_R(n)$  of  $n$  Rydberg excitations (open bars) and the mean number of excitations  $\langle n_R \rangle$ . Also shown is the Poisson distribution  $p_{\text{Poisson}}(n)$  for the same  $\langle n_R \rangle$  (solid brown circles). (c1-c4) Average spatial distributions of  $n$  Rydberg excitations, corresponding to two largest  $p_R(n)$  in (b1-b4), after centering and aligning each configuration  $\{\hat{\sigma}_{rr}^j\}_n$ , and the corresponding axial  $P(\rho)$  and angular  $P(\phi)$  probability distributions [ $P(\rho)$  are binned over the lattice spacing  $a$  and  $P(\phi)$  are binned over the interval  $\pi a/d$ ].

berg excitations in the cloud  $\langle n_R \rangle = \sum_n n p_R(n)$  and the probabilities  $p_R(n)$  to find  $n = 0, 1, 2, \dots$  excitations. Interestingly,  $\langle n_R \rangle$  grows with the size of the system as  $\langle n_R \rangle \propto (d/d_b)^{5/3}$  [Fig. 2(a)], rather than  $(d/d_b)^2$  as one might expect for a 2D bulk system. This is a finite-size effect, due to the concentration of the mutually repelling Rydberg excitations at the boundary of the cloud.

To quantify the number distribution of Rydberg excitations, we use the Mandel  $Q$  parameter [50]

$$Q \equiv \frac{\langle n_R^2 \rangle - \langle n_R \rangle^2}{\langle n_R \rangle} - 1, \quad (2)$$

where  $\langle n_R^2 \rangle = \sum_n n^2 p_R(n)$ . A Poissonian distribution  $p_{\text{Poisson}}(n) = \langle n_R \rangle^n e^{-\langle n_R \rangle}/n!$  would lead to  $Q = 0$ , while  $Q < 0$  corresponds to sub-Poissonian distribution, with  $Q = -1$  attained for a definite number  $n$  of excitations. We find highly sup-Poissonian distribution of  $p_R(n)$ , Figs. 1(b1-b4), and nearly constant  $Q \simeq -0.84 \forall d > d_b$ ,

Fig. 2(b). Note that in the absence of coherence realization,  $\Gamma_z = 0$ , the (classical) correlations of the Rydberg excitations are considerably smaller,  $Q \sim -0.5$ , as was shown in [54].

Next, for each  $d$ , we select the values of  $n$  with the largest probabilities  $p_R(n)$  (frequent occurrence) and analyze the average spatial distribution of the corresponding configurations  $\{\hat{\sigma}_{rr}^j\}_n$  containing precisely  $n$  Rydberg excitations, as was done in [29]. To this end, for each configuration  $\{\hat{\sigma}_{rr}^j\}_n$  we set the origin of the polar coordinate system at the center of mass (CoM) of the excitations. We then determine the mean angle of the position vectors of all the excited atoms with respect to a reference ( $x$ ) axis and rotate the configuration about the origin by that angle. The averages over many thus centered and aligned configurations are shown in Figs. 1(c1-c4). Below each 2D density plot (apart from that for  $n = 1$ ) we also show the corresponding axial  $P(\rho)$  and angular  $P(\phi)$  probability distributions of the  $n$  excitations. We observe

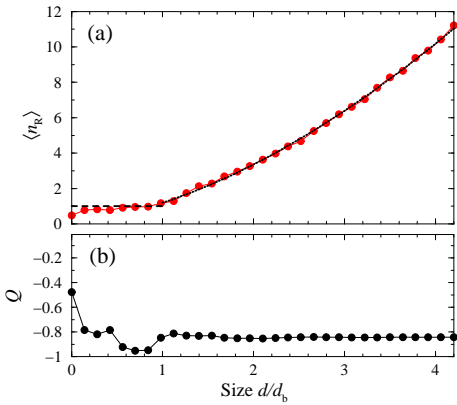


FIG. 2. (a) Mean number of Rydberg excitations  $\langle n_R \rangle$ , and (b) the corresponding  $Q$  parameter vs the system size  $d/d_b$ . In (a) the black dashed line for  $d < d_b$  is  $\langle n_R \rangle = 1$ , and the dotted line for  $d \geq d_b$  is  $\langle n_R \rangle = 0.2 + (d/d_b)^{1.66}$ .

that the Rydberg excitations tend to arrange in regular spatial patterns, i.e., they crystallize. For a small cloud,  $d \lesssim 2d_b$ , the  $n$  excitations are pushed to the boundary, and their angular separation is  $\delta\phi \sim 2\pi/n$ . But already for  $d \sim 3d_b$  we encounter a significant probability of Rydberg excitation at the cloud center, while for  $d \sim 4d_b$  we clearly observe a double peak structure of  $P(\rho)$ , with the largest peak close to the boundary of the cloud and the smaller peak corresponding to the inside ring of the corresponding 2D density plot. The distance between the two peaks of  $P(\rho)$  is somewhat larger than the blockade distance  $d_b$  (see below).

In Fig. 3 we plot the normalized spatial correlations

$$g^{(2)}(z) \equiv \frac{\sum_{i \neq j} \delta_{z, z_{ij}} \bar{\sigma}_{rr}^i \bar{\sigma}_{rr}^j}{\sum_{i \neq j} \delta_{z, z_{ij}} \bar{\sigma}_{rr}^i \bar{\sigma}_{rr}^j}, \quad (3)$$

where  $\delta_{z, z_{ij}}$  is the Kronecker delta which selects the pairs of atoms  $i, j$  at distance  $z_{ij} = z$ . Clearly, at short distances  $z < d_b$  the Rydberg excitations avoid each other [27–29], while at  $z_{\max}$  slightly larger than  $d_b$ , there is a pronounced maximum of  $g^{(2)}(z)$ , which implies higher probability of finding pairs of Rydberg excitations separated by distance  $z_{\max}$ . Precisely this suppression, or blockade, of Rydberg excitations at shorter

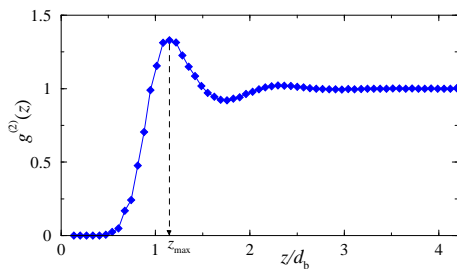


FIG. 3. Correlations of Rydberg excitations  $g^{(2)}(z)$  vs distance  $z$ ; the maximum is at  $z_{\max} = 1.15d_b$ .

distances, and the elevated probability of excitations at distance  $z_{\max}$ , are responsible for the observed quasi-crystallization and inner shell structure of the spatial distribution of  $\bar{\sigma}_{rr}^j$ . At longer distances  $z > d_b$ , the correlation function  $g^{(2)}(z)$  exhibits strongly damped spatial oscillations, signifying the absence of a long-range order. Similar results were obtained for a 1D system in [49], where it was found that the correlation length  $\xi$  exceeding the oscillation period  $\lambda \gtrsim d_b$  can only be attained at high atomic densities (thirty or more atoms per blockade distance  $d_b$ ).

#### IV. CONCLUDING REMARKS

To summarize, we have studied the steady-state distribution of Rydberg excitations in a 2D cloud of atoms subject to continuous resonant driving. The main results of this study are a very narrow (sub-Poissonian) distribution of the number of excitations within the system and the formation of regular spatial structures of Rydberg excitations, which was interpreted via the characteristic form of the pair-correlation function of the excitations.

We note that the sub-Poissonian statistics of the number of Rydberg excitations and the corresponding negative values of the Mandel  $Q$  parameter were observed in several experiments [30–32], while the spatial ordering of  $n \leq 5$  Rydberg excitations in a 2D optical lattice was impressively demonstrated in [29]. These experiments and the accompanying theoretical/numerical calculations dealt with the transient unitary dynamics of the system. In contrast, the present study is an attempt at a detailed characterization of the stationary state of a dissipative many-body system.

Let finally us discuss the limitations of our approach and the obtained results. The two key questions are whether the steady state can be attained in a real cold-atom experiment, especially for a large ensemble of  $N \sim 10^3$  atoms, and to what extend the employed semiclassical treatment is adequate to describe the true steady state of the system. These questions were addressed in [54], at least for a moderate number of atoms  $N \lesssim 50$ , and here let us briefly summarize the conclusions. In an experiment with typical relaxation rates of the atoms [29], the time scale for attaining the true many-body steady state is tens of  $\mu\text{s}$ —or more for larger  $N$ —which can be prohibitively long due to the loss of atoms and the need of continuous laser irradiation. However, already after several  $\mu\text{s}$  of laser driving, the spatial probability distribution of Rydberg excitations ceases to change appreciably [29] being close to the steady-state distribution [54]. This is particularly true for strong coherence relaxation  $\Gamma_z \gtrsim \Omega$  which quickly dephases the atoms rendering the system essentially classical but still strongly correlated [54]. The results of the semiclassical Monte Carlo simulations are then trustworthy, as was demonstrated in [49] (see also [32, 51–53]).

---

[1] I. Bloch, J. Dalibard, and W. Zwerger, *Rev. Mod. Phys.* **80**, 885 (2008); M. Lewenstein, A. Sanpera, V. Ahufinger, B. Damski, A. Sen De, and U. Sen, *Adv. Phys.* **56**, 243 (2007).

[2] D. Jaksch, C. Bruder, J.I. Cirac, C.W. Gardiner, and P. Zoller, *Phys. Rev. Lett.* **81**, 3108 (1998); M. Greiner, O. Mandel, T. Esslinger, T.W. Hänsch, and I. Bloch, *Nature* **415**, 39 (2002); D. Jaksch and P. Zoller, *Ann. Phys. (N.Y.)* **315**, 52 (2005).

[3] S. Fölling, S. Trotzky, P. Cheinet, M. Feld, R. Saers, A. Widera, T. Müller, and I. Bloch, *Nature* **448**, 1029 (2007); S. Trotzky, P. Cheinet, S. Fölling, M. Feld, U. Schnorrberger, A.M. Rey, A. Polkovnikov, E.A. Demler, M.D. Lukin, and I. Bloch, *Science* **319**, 295 (2008).

[4] A.B. Kuklov and B.V. Svistunov, *Phys. Rev. Lett.* **90**, 100401 (2003); L.-M. Duan, E. Demler, and M.D. Lukin, *Phys. Rev. Lett.* **91**, 090402 (2003).

[5] D. Petrosyan, B. Schmidt, J. R. Anglin and M. Fleischhauer, *Phys. Rev. A* **76**, 033606 (2007); B. Schmidt, M. Bortz, S. Eggert, M. Fleischhauer and D. Petrosyan, *Phys. Rev. A* **79**, 063634 (2009).

[6] T. Lahaye, C. Menotti, L. Santos, M. Lewenstein, and T. Pfau, *Rep. Prog. Phys.* **72** 126401 (2009).

[7] T.F. Gallagher, *Rydberg Atoms* (Cambridge University Press, Cambridge, 1994).

[8] M. Saffman, T.G. Walker, and K. Mølmer, *Rev. Mod. Phys.* **82**, 2313 (2010); D. Comparat and P. Pillet, *J. Opt. Soc. Am. B* **27**, A208 (2010).

[9] R. Löw, H. Weimer, J. Nipper, J.B. Balewski, B. Butscher, H.P. Büchler, and T. Pfau, *J. Phys. B* **45**, 113001 (2012).

[10] J.E. Johnson and S.L. Rolston, *Phys. Rev. A* **82**, 033412 (2010).

[11] N. Henkel, R. Nath, and T. Pohl, *Phys. Rev. Lett.* **104**, 195302 (2010).

[12] G. Pupillo, A. Micheli, M. Boninsegni, I. Lesanovsky, and P. Zoller, *Phys. Rev. Lett.* **104**, 223002 (2010).

[13] A. Lauer, D. Muth and M. Fleischhauer, *New J. Phys.* **14** 095009 (2012).

[14] D. Tong, S.M. Farooqi, J. Stanojevic, S. Krishnan, Y.P. Zhang, R. Côté, E.E. Eyler, and P.L. Gould, *Phys. Rev. Lett.* **93**, 063001 (2004).

[15] T. Vogt, M. Viteau, J. Zhao, A. Chotia, D. Comparat, and P. Pillet, *Phys. Rev. Lett.* **97**, 083003 (2006).

[16] K. Singer, M. Reetz-Lamour, T. Amthor, L.G. Marcassa, and M. Weidemüller, *Phys. Rev. Lett.* **93**, 163001 (2004).

[17] R. Heidemann, U. Raitzsch, V. Bendkowsky, B. Butscher, R. Löw, L. Santos, and T. Pfau, *Phys. Rev. Lett.* **99**, 163601 (2007).

[18] R. Löw, H. Weimer, U. Krohn, R. Heidemann, V. Bendkowsky, B. Butscher, H.P. Büchler, and T. Pfau, *Phys. Rev. A* **80**, 033422 (2009).

[19] M. Robert-de-Saint-Vincent, C.S. Hofmann, H. Schempp, G. Günter, S. Whitlock, and M. Weidemüller, *Phys. Rev. Lett.* **110**, 045004 (2013).

[20] M.D. Lukin, M. Fleischhauer, R. Côté, L.M. Duan, D. Jaksch, J.I. Cirac, and P. Zoller, *Phys. Rev. Lett.* **87**, 037901 (2001).

[21] F. Robicheaux and J.V. Hernandez, *Phys. Rev. A* **72**, 063403 (2005).

[22] J. Stanojevic and R. Côté, *Phys. Rev. A* **80**, 033418 (2009).

[23] E. Urban, T.A. Johnson, T. Henage, L. Isenhower, D.D. Yavuz, T.G. Walker, and M. Saffman, *Nature Phys.* **5**, 110 (2009); A. Gaëtan, Y. Miroshnychenko, T. Wilk, A. Chotia, M. Viteau, D. Comparat, P. Pillet, A. Browaeys, and P. Grangier, *ibid* **5**, 115 (2009).

[24] Y.O. Dudin, L. Li, F. Bariani, and A. Kuzmich, *Nature Phys.* **8**, 790 (2012).

[25] D. Petrosyan and K. Mølmer, *Phys. Rev. A* **87**, 033416 (2013).

[26] C. Ates, I. Lesanovsky, C.S. Adams, and K.J. Weatherill, *Phys. Rev. Lett.* **110**, 213003 (2013).

[27] A. Schwarzkopf, R.E. Sapiro, and G. Raithel, *Phys. Rev. Lett.* **107**, 103001 (2011).

[28] M. Viteau, M.G. Bason, J. Radogostowicz, N. Malossi, D. Ciampini, O. Morsch, and E. Arimondo, *Phys. Rev. Lett.* **107**, 060402 (2011).

[29] P. Schauß, M. Cheneau, M. Endres, T. Fukuhara, S. Hild, A. Omran, T. Pohl, C. Gross, S. Kuhr, and I. Bloch, *Nature* **491**, 87 (2012).

[30] T. Cubel Liebisch, A. Reinhard, P.R. Berman, and G. Raithel, *Phys. Rev. Lett.* **95**, 253002 (2005).

[31] M. Viteau, P. Huillery, M.G. Bason, N. Malossi, D. Ciampini, O. Morsch, E. Arimondo, D. Comparat, and P. Pillet, *Phys. Rev. Lett.* **109**, 053002 (2012).

[32] C.S. Hofmann, G. Günter, H. Schempp, M. Robert-de-Saint-Vincent, M. Gärttner, J. Evers, S. Whitlock, and M. Weidemüller, *Phys. Rev. Lett.* **110**, 203601 (2013).

[33] H. Weimer, R. Löw, T. Pfau, and H.P. Büchler, *Phys. Rev. Lett.* **101**, 250601 (2008).

[34] H. Weimer and H.P. Büchler, *Phys. Rev. Lett.* **105**, 230403 (2010).

[35] T. Pohl, E. Demler, and M.D. Lukin, *Phys. Rev. Lett.* **104**, 043002 (2010).

[36] J. Schachenmayer, I. Lesanovsky, A. Micheli, and A.J. Daley, *New J. Phys.* **12**, 103044 (2010).

[37] R.M.W. van Bijnen, S. Smit, K.A.H. van Leeuwen, E.J.D. Vredenbregt, and S.J.J.M.F. Kokkelmans, *J. Phys. B* **44**, 184008 (2011).

[38] E. Sela, M. Punk, and M. Garst, *Phys. Rev. B* **84**, 085434 (2011).

[39] I. Lesanovsky, *Phys. Rev. Lett.* **106**, 025301 (2011).

[40] I. Lesanovsky, *Phys. Rev. Lett.* **108**, 105301 (2012).

[41] M. Gärttner, K.P. Heeg, T. Gasenzer and J. Evers, *Phys. Rev. A* **86**, 033422 (2012).

[42] W. Zeller, M. Mayle, T. Bonato, G. Reinelt, and P. Schmelcher, *Phys. Rev. A* **85**, 063603 (2012).

[43] T.E. Lee, H. Häffner, and M.C. Cross, *Phys. Rev. A* **84**, 031402(R) (2011).

[44] J. Qian, G. Dong, L. Zhou, and W. Zhang, *Phys. Rev. A* **85**, 065401 (2012).

[45] M. Höning, D. Muth, D. Petrosyan, and M. Fleischhauer, *Phys. Rev. A* **87**, 023401 (2013).

[46] S. Ji, C. Ates and I. Lesanovsky, *Phys. Rev. Lett.* **107**, 060406 (2011).

[47] C. Ates, J. P. Garrahan and I. Lesanovsky *Phys. Rev. Lett.* **108**, 110603 (2012).

[48] C. Ates and I. Lesanovsky, *Phys. Rev. A* **86**, 013408 (2012); S. Ji, C. Ates, J.P. Garrahan and I. Lesanovsky, *J. Stat. Mech.* P02005 (2013).

[49] D. Petrosyan, M. Höning, and M. Fleischhauer, *Phys.*

Rev. A **87**, 053414 (2013).

[50] L. Mandel, Opt. Lett. **4**, 205 (1979).

[51] K.P. Heeg, M. Gärttner and J. Evers, Phys. Rev. A **86**, 063421 (2012).

[52] C. Ates, T. Pohl, T. Pattard, and J.M. Rost, Phys. Rev. A **76**, 013413 (2007).

[53] C. Ates, S. Sevinçli, and T. Pohl, Phys. Rev. A **83**, 041802(R) (2011).

[54] D. Petrosyan, arXiv:1305.2341.

[55] P. Lambropoulos and D. Petrosyan, *Fundamentals of Quantum Optics and Quantum Information*, (Springer, Berlin, 2007).

[56] K. Singer, J. Stanojevic, M. Weidemüller, and R. Côté, J. Phys. B **38**, S295 (2005).